

Universal nature of collective plasmonic excitations in finite 1-D carbon-based nanostructures

Eric Polizzi* and Sigfrid Yngvesson

Department of Electrical and Computer Engineering, University of Massachusetts, Amherst

(Dated: September 25, 2021)

Tomonaga-Luttinger (T-L) theory predicts collective plasmon resonances in 1-D nanostructure conductors of finite length, that vary roughly in inverse proportion to the length of the structure. In-depth quantitative understanding of such resonances which have not been clearly identified in experiments so far, would be invaluable for future generations of nano-photonic and nano-electronic devices that employ 1-D conductors. Here we provide evidence of the plasmon resonances in a number of representative 1-D finite carbon-based nanostructures using first-principle computational electronic spectroscopy studies. Our special purpose real-space/real-time all-electron Time-Dependent Density-Functional Theory (TDDFT) simulator can perform excited-states calculations to obtain correct frequencies for known optical transitions, and capture various nanoscopic effects including collective plasmon excitations. The presence of 1-D plasmons is universally predicted by the various numerical experiments, which also demonstrate a phenomenon of resonance splitting. For the metallic carbon nanotubes under study, the plasmons are expected to be related to the T-L plasmons of infinitely long 1-D structures.

PACS numbers:

Keywords: 1-D conductors, nanoplasmonics, real-time TDDFT, computational electronic spectroscopy, Tomonaga-Luttinger liquid, plasmon velocity

I. INTRODUCTION

Nanoplasmonics is a field that has grown rapidly in the last few years [1, 2]. Covering a range from terahertz through infrared to visible light frequencies, this field already offers numerous applications to electronics and photonics. In the visible and Near IR (NIR) range, nano-antennas [3] and nanoparticles have provided drastically enhanced coupling to electromagnetic waves [4]. All of this research work has taken advantage of plasmonic surface modes - either on nanoparticles, or on metallic sheets - and has led to some initial practical applications. However, there are still significant fundamental limitations that must be overcome for further progress to be possible in this field [5]. While there is an extensive literature on 1-D plasmons, these have not been emphasized for applications due to the difficulty of preparing devices and performing experiments. Yet, 1-D conductors are of interest since they can potentially exhibit lower losses than the 2-D ones. The chief signature of 1-D plasmons is a high-frequency excitation (i.e. energy resonance) that depends inversely on the length of the conductor. Examples of nano-structures that can support 1-D plasmons are graphene nanoribbons (GNRs), single wall carbon nanotubes (SWCNTs) and linear carbon chains. Due to the very strong coulomb interactions in such 1-D systems, the low-energy excitations of interacting electrons cannot be adequately described by Landau's Fermi liquid theory [6], which has to be replaced by Tomonaga-Luttinger (T-L) liquid theory [7–10]. Specifically, it was shown that

metallic carbon nanotubes can be well described with the T-L theory [11, 12]. A bosonized representation of the Hamiltonian led to the following conclusions: (i) the density of single particle states is a power function of the energy and vanishes at the Fermi energy; (ii) consistent with (i) the conductance of electrons tunneling into the CNT has a universal power law dependence on voltage and temperature; (iii) the electron states are separated into charge states and spin states [13]. In the simulations that follow spin/charge separation effects are neglected; (iv) collective boson states form charge density waves in the CNT (“T-L plasmons”) which propagate with a velocity $v_P = v_F/g$ where v_F is the Fermi velocity $\simeq 1 \times 10^6 m/s$, [14] and g is a parameter that depends on the strength of the Coulomb interaction and on screening by the electrostatic environment (the latter being a weak effect) [12]. The predictions (i) and (ii) have been well verified by transport [15, 16] and optical [17] measurements. The parameter g is < 1 for T-L liquids and $= 1$ for Fermi liquids, v_P is thus higher than v_F . An average plasmon velocity of the predicted magnitude was recently deduced from absorption measurements on enriched SWCNTs films [18]. Ultra-fast time-dependent measurements evidenced ballistic electron oscillations in isolated SWCNTs, but the propagation velocity was equal to the Fermi velocity, consistent with single particle excitations, not plasmons [19]. Detailed experimental confirmation of the predicted plasmon resonance frequencies in isolated SWCNTs is thus still an unsolved problem. Estimates of g for CNTs yield values in the range $0.26 - 0.33$ [12] resulting in v_P being in the range $3 - 4 \times 10^6 m/s$. Electromagnetic simulations have yielded v_P up to $6.2 \times 10^6 m/s$ [20]. Recently, T-L liquid behavior with $g = 0.53$ was verified in atomic gold chains by tunneling and optical measurements [21].

*Electronic address: polizzi@ecs.umass.edu

The focus of this paper is the dynamic behavior of the collective medium in 1-D conductors and its resonances. A physical picture of the resonances can be gained by realizing the equivalence of the finite length 1-D conductor to a transmission line [22, 23]. The T-L plasmon waves resonate as they are reflected at the ends of the conductor and the fundamental resonance frequency will be given by $f = v_p/(2L)$ [24] where L is the length of the conductor. Single quasi-particles similarly resonate at $f = v_F/(2L)$. In our simulations we explore both of these types of resonances as well others that will be discussed in the text.

First-principle calculations are becoming critical to provide evidence of plasmon resonances in 1-D carbon-based nanostructures. Such quantitative simulations are known to be challenging, since they should be both capable to provide reliable information on the many-body excited states (beyond ground state theory), and to address large-scale computational needs of finite dimensional systems (beyond the solid-state unit-cell). The time dependent density functional theory (TDDFT) [25] alongside with the simple adiabatic local density approximation (ALDA) for the many-body exchange-correlation term, has been very successful for providing accurate absorption spectra of a large number of complex molecular systems [26]. The real-time TDDFT approach introduced by Yabana and Bertsch [27, 28], in particular, combines both potential for parallel computing scalability, and an intuitive treatment of the real-time spectroscopy that can deal with any form of excitations. Our in-house simulator, named NESSIE, is performing both all-electron real-space DFT ground state and real-time TDDFT excited states calculations. NESSIE benefits from the high-performance capabilities of the FEAST eigensolver [29, 30], which has also allowed to efficiently redesign various stages of the electronic structure numerical modeling process [31–33]. Detailed information on our numerical real-space and real-time modeling framework is provided within the supporting document of this article.

Two types of real-time TDDFT simulations are considered in our experiments. First, the spectroscopic information is obtained from linear response calculations after a short and weak polarized impulse is applied along the longitudinal or perpendicular direction of the 1-D nanostructure. Then, once resonances of interest are identified in the absorption spectrum, new time-dependent calculations are performed in response to a realistic stimulus, such as a laser tuned to each resonance frequency (e.g. sinusoidal excitation along the longitudinal direction). Such simulations aim at providing more detail on the 3-D electron dynamics of the particular resonances with relevant information about their nature. From atom and benzene-like chain structures to short carbon nanotubes, our numerical experiments discussed below progressively account for an increase in the physical and computational complexities of the 1-D atomic structure.

II. CARBYNE

Carbyne is a chain of carbon atoms that comprises either double or alternating single and triple atomic bonds. With recent progress in synthesis [34], first-principle theoretical investigations have become increasingly more relevant to study the various attractive physical properties of this material [35]. Previous studies of carbon chains using the TDDFT approach have been reported in Refs. [36–38]. Our numerical simulations of NC_{2n}N shown in Figure 1, are in good agreement with the experimental data found in Ref. [39], where the strong longitudinal resonance shifts progressively towards the left of the spectrum with longer chains (i.e. red shift). Their oscillator strength increases with the length of the chain indicating that more electrons can participate in the plasmonlike collective excitations. Furthermore, the associated velocity of the resonances is in the typical range of collective plasmons (as discussed further). References [36, 38] also identify these excitations as collective plasmons. We note that the carbynes are not metallic and thus are not expected to conform with the T-L theory. Nevertheless, carbynes show strong 1-D Plasmon excitations. Moreover, our results show that these longitudinal resonances do not appear with a perpendicular excitation (see the NC_8N plot at the top of Figure 1). In contrast, one can identify other small resonances for instance, at 11.01eV, and at 14.68eV which do not depend on the length of the chain. These particular energy transitions are comparatively close to the ionization potentials of the local atoms C and N, respectively at 11.26eV and 14.53eV [40].

The longitudinal resonances can be observed in more detail in Figure 2 (left plot) for the NC_{16}N , HC_{16}H , and HC_{24}H chains. We note that the spectra produced for the C_{16} chain using the H or N termination are very similar. Our results are also quantitatively close to the ones obtained in Ref. [38] for the HC_{2n}H chain that makes use of the projector augmented-wave (PAW) pseudopotential and performs TDDFT linear response simulations in the frequency domain. The lowest energy plasmon resonances found in these results are also in agreement with earlier real-time TDDFT simulations performed in Ref. [37] using a smooth pseudopotential. In comparison with the latter however, both the PAW and our full-core potential treatments reveal additional plasmonlike resonances at higher energies. These oscillations can be observed in the experimental data of the NC_nN chains [39]. In our simulations, the splitting between these resonances becomes narrower for the HC_{24}H and only two main peaks can be observed instead of three for HC_{16}H . The isosurface snapshot plots in Figure 2 represent three additional real-time TDDFT simulation results that can help provide more insights on the time-dependent electron dynamics of the plasmonic resonances in HC_{16}H . The strongest

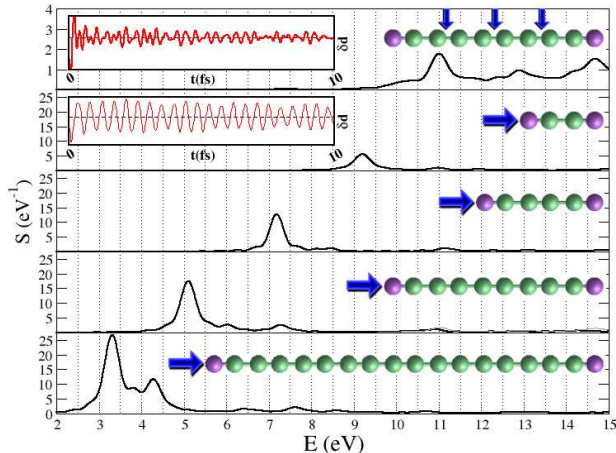


FIG. 1: Computed absorption spectra of NC_{2n}N with lengths $n = 1, 2, 4, 8$ (using the single-triple bond alternation structure and the optimized geometries reported in Ref. [41]). The plot on the top for $n = 4$ is associated with the perpendicular response of a weak impulse applied along the same direction. All the other plots consider the response of an excitation applied along the longitudinal direction of the chain. The figure insets illustrate the variation of the induced dipole obtained from our real-time TDDFT calculations and that are used to derive the absorption spectra of the corresponding structures.

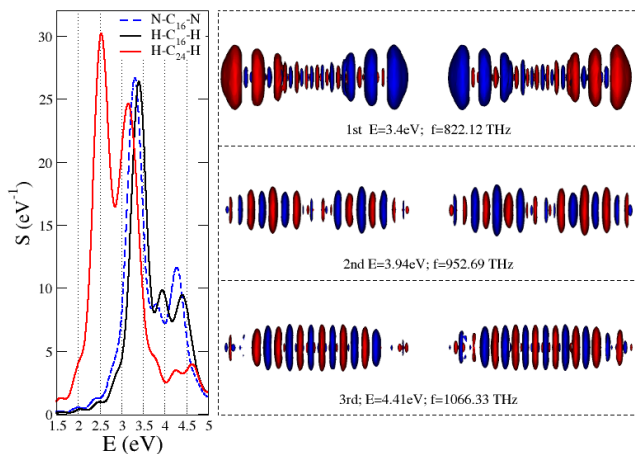


FIG. 2: The left plot includes a more detailed representation of the main resonances of NC_{16}N observed in Fig. 1; it is also plotted alongside with the absorption spectra of the H-terminated carbon chains HC_{24}H and HC_{16}H (using the optimized geometries reported in Ref. [42]). The latter counts three longitudinal resonances at 3.4eV, 3.94eV and 4.41eV. After new excitations of the structure at each one of these specific energy transitions (i.e. sinusoidal excitation at specific frequencies), the figures on the right represent the 4D isosurface snapshots of the charge oscillation (i.e. the deviation of the charge density from the ground state – positive and negative deviations respectively in red and blue) all taken at a different time of the simulation where the dipole goes through a maximum and a minimum, respectively.

resonance at the lowest energy transition gives rise to a distinguishable plasmon that can oscillate back and forth along the longitudinal direction. This collective particle excitation likely takes place within the first Van Hove singularity of the 1-D structure where the electrons are strongly coupled. It has the signature of a plasmon with a calculated velocity of $v_{pl} = 3.18 \times 10^6 \text{m/s}$ which increases to $v_{pl} = 3.64 \times 10^6 \text{m/s}$ for HC_{24}H . The results for the other two snapshot plots confirm the presence of additional longitudinal resonance modes that were mentioned in Ref. [38], with cosine and sine like envelope features for the plasmonic excitations. These two excitations have a different character in that the charge density alternates from positive to negative for each atom pair, analogous to optical phonon modes. Finally, we note that no single particle excitation at the Fermi velocity is observed since the carbon chain family considered here is semiconducting.

III. ACENES AND POLY(P-PHENYLENE)

Acenes and Poly(p-phenylene) (PPP) are polycyclic aromatic hydrocarbons consisting of linear benzene rings that are respectively fused or attached. They can also be thought of as the narrowest graphene nanoribbons (GNR) of finite lengths, associated with the zig-zag configuration for acenes (2-ZGNR) and the armchair one for PPP (3-AGNR). Understanding the properties of long acenes in particular, is the subject of active research [43].

Results for anthracene, tetracene and pentacene reported in Figure 3 confirm that the strong longitudinal UV resonances along the z-direction that appear respectively at 4.85eV, 4.30eV, 3.88eV, are in remarkable agreement with the experimental data in Ref. [45]. While TDDFT using traditional exchange-correlation functionals such as ALDA fail to describe the important low-lying excited states in acene compounds [44], it appears capable to accurately capture the main nanoscopic effects. These resonances are plasmonlike, since we note a progressive shift towards the left of the spectrum with longer chains accompanied by an increase in oscillator strength. They are also absent from the results of excitations along the x and y directions. For the latter, in turn, one can identify two other resonances that stay independent of the chain length, at 11.22eV using an x-polarized impulse that equally excites all the carbon atoms in the y - z plane (energy relatively close to the ionization potential of C), and at 7.55eV using an y-polarized impulse that equally excites all the individual fused benzene rings (energy relatively close to the $\pi \rightarrow \pi^*$ transition in benzene). For the case of pentacene, in addition to a strong plasmon resonance at 3.88eV, we note a couple of weaker longitudinal resonances at 4.84eV and 5.25eV (see top right plot of Figure 3). The latter comes close to the experimental HOMO-LUMO gap at 5.2eV [46] (this gap is known to be severely underestimated by DFT at $\sim 1\text{eV}$). The

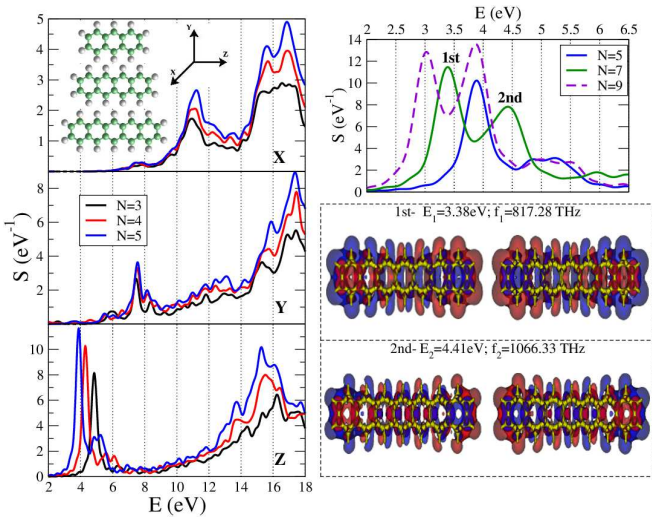


FIG. 3: The left plots present the computed absorption spectra of anthracene ($N=3$), tetracene ($N=4$), pentacene ($N=5$) associated with the responses of weak impulses separately applied along the three main directions (regular bond lengths are used for the geometries: $l_{C-C} = 1.42\text{\AA}$ and $l_{C-H} = 1.09\text{\AA}$). The top right plot focuses on the plasmonic response of an excitation along the longitudinal direction for pentacene ($N=5$), heptacene ($N=7$) and nonacene ($N=9$). The heptacene, in particular, counts two main resonances at 3.38eV and 4.41eV. The 4D isosurface snapshots represent the charge oscillations associated with these two energy transitions obtained at different simulation times where the dipole response reaches a maximum and a minimum.

results on heptacene and nonacene in Figure 3, clearly show that as the length of the structure increases, a second strong resonance appears. The isosurface snapshots representing the electron dynamics for the two main resonances of heptacene confirm the presence of two plasmons. In contrast to the case of carbon chains, this second resonance does not result from an additional longitudinal confinement mode, and the results indicate the presence of another channel (i.e. two confinement modes are then present in the transverse x, y plane). We note that similar double plasmon resonances have also been recently observed using semi-empirical simulations applied to GNR structures with variable widths [47]. The calculated plasmon velocities associated with the first and second resonances of heptacene, $v_{pl_1} = 2.77 \times 10^6 m/s$ and $v_{pl_2} = 3.61 \times 10^6 m/s$, increase to $v_{pl_1} = 3.18 \times 10^6 m/s$ and $v_{pl_2} = 4.08 \times 10^6 m/s$ for nonacene.

The case of finite PPP is shown in Figure 4 using lengths of 5 and 10 unit cells. Excitations along the perpendicular directions (including the x-direction not shown here) provides results comparable to the ones obtained for acenes in Figure 3. However, we note one additional resonance at around 6.55eV for an excitation along the y perpendicular direction (curve denoted '5T') which is also present (and amplified) with an excitation along the longitudinal z direction for both

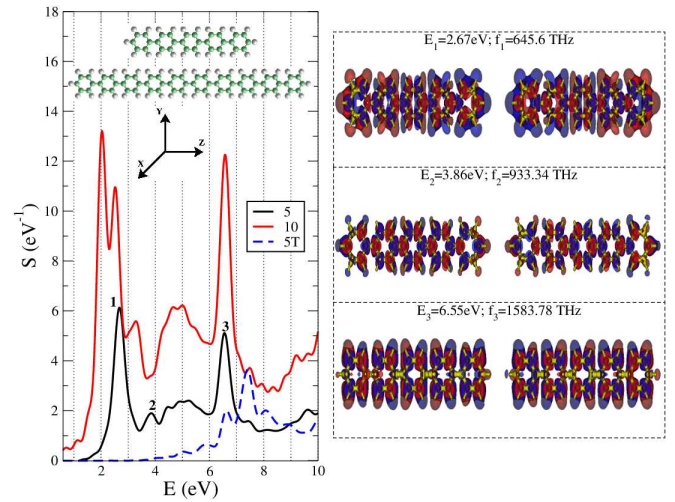


FIG. 4: The left plot presents the computed absorption spectra of a finite PPP with 5 and 10 unit cells (using the geometries reported in Ref. [48]), obtained after excitations along the z longitudinal or y perpendicular direction. The result for the latter is noted 5T (for the 5 unit cells). The 4D isosurface snapshots on the right represent the charge oscillations associated with three main selected longitudinal resonances of the 5 unit cell PPP.

5 and 10-PPP. All the other longitudinal resonances at lower energies are absent from the '5T' curve. The isosurface snapshots of the charge oscillations, provide some useful information on the nature of the three main selected longitudinal resonances for 5-PPP. The strong first peak can be associated with a plasmon, while the second and third peaks reveal different characteristics related to "band-to-band" transitions. In particular, the second peak shifts from 3.86eV to 3.3eV for the long 10-PPP which is in very good agreement with the strong experimental absorption peak (related to the bandgap) found at 3.4eV for PPP [49]. The position of the third peak, in turn, is not sensitive to variation in length. A closer look at the isosurface plots show that the charge oscillations at 6.55eV are somehow localized within each attached benzene ring. We note that a broader "band-to-band" transition region appears at around 5eV for both 5 and 10-PPP. Finally, the main plasmon resonance at 2.67eV i.e. $v_{pl} = 2.44 \times 10^6 m/s$ shifts towards the left of the spectrum of the 10-PPP and, similarly to the case of long acene, splits into two peaks. The calculated plasmon velocities associated with the two resonances are $v_{pl_1} = 3.97 \times 10^6 m/s$ and $v_{pl_2} = 4.83 \times 10^6 m/s$.

IV. SINGLE-WALL CARBON NANOTUBE (SWCNT)

Figure 5 shows our results for simulations of a finite (3,3) armchair SWCNT. To stabilize the structure one

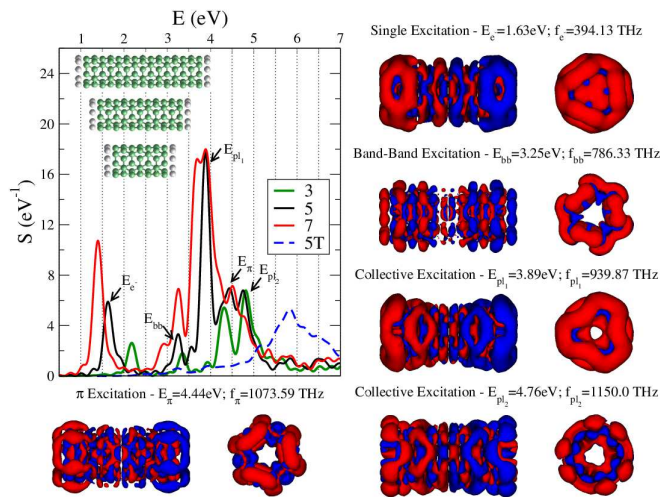


FIG. 5: The computed absorption spectra of the finite (3,3) armchair SWCNT with three different length 3, 5 and 7 unit cells (the C-C bond length is fixed at 1.44\AA and one additional carbon ring of type 'A' is added to the structures e.g. 'H-AB-AB-AB-A-H' for the 3 unit cells with Hydrogen termination). The '5T' curve indicates the result from an excitation in the perpendicular direction, all other results consider an excitation along the longitudinal direction of tube. The 4D isosurface snapshots on the right and below the spectrum represent the charge oscillations associated with five main selected longitudinal resonances of the 5 unit cell tube. They have all been taken at a different time of the simulation where the dipole goes through a maximum, and the figures include both side and edge views of the nanotube.

additional carbon ring, and hydrogen atoms were added at the ends. The H atoms are expected to have only minor effects on the resonances observed. Armchair SWCNTs are known to exhibit metallic conduction [14] and, as mentioned in the introduction, they can be described by the T-L theory in the infinite length limit [11, 12]. We simulated tubes of three different lengths, 3, 5, and 7 "unit cells", respectively. The simulations were performed for an E-field parallel to the z-axis of the tubes (the long axis), marked '3', '5' and '7', as well as perpendicular to that axis (for the 5 unit cell case, marked '5T'). We first distinguish resonances that do not change with the length (L) of the tube. The peak at about 4.44eV can be identified as being due to the π -plasmon (E_π in the Figure). Note the characteristic distribution of the oscillating charges, following the bonds, in the snapshot displayed below the spectra. A broad band with a peak at $\sim 15\text{eV}$ due to the $\pi + \sigma$ plasmon can also be observed in the spectra (observations are included in the supporting information document). Since the above plasmons are basically of the bulk (3-D) type, they can also be excited by a field in the direction perpendicular to the tube. Both of these resonances are well known for SWCNTs and have been detected experimentally by Electron Energy Loss (EEL) spectroscopy [50] as well as by optical spectroscopy (the π -plasmon) [51, 52]. We note that

the π -plasmon resonance for perpendicular excitation is shifted to a higher energy, 5.8eV, in qualitative agreement with the experimental data. The π -plasmon resonance for the 3 unit cell case is not so easy to identify, see further discussion below. There is also a resonance for all values of L at about 3.25eV (E_{bb} in Figure 5). This resonance energy agrees with experimental optical data and simulations [51, 53] and can be identified as a "band-to-band" resonance for infinitely long tubes and for higher energy bands. The simulations show that this peak does not vary with L, and also that it can not be excited perpendicular to the axis, as expected for a band-to band transition. The charge distribution under sinusoidal excitation shown in Figure 5 clearly lacks the collective character evident in the plasmon resonances.

One type of resonance that does vary with L occurs in the lowest energy range, from about 1.4 to 2.2eV (E_{e-} in the Figure). Calculating a velocity for this resonance we find a value $0.98 \times 10^6\text{m/s}$ and $1.18 \times 10^6\text{m/s}$ respectively for the 5 and 7 unit cell cases, which is close to the Fermi velocity. We note that this resonance can only be excited by a field parallel to the tube axis, as expected if it is due to electrons resonating from one end of the tube to the other. This is the type of single particle excitation resonance that was measured in Ref. [19]. Further evidence for this interpretation is obtained by inspecting the top 4-D isosurface snapshots to the right of the spectra ('Single Excitation - $E_{e-} = 1.63\text{eV}$ '), which show the periodic oscillation of the charge density.

Finally, we find two strong peaks at energies of 3.69 – 3.89eV (a split peak for the longest tube) and 3.89eV (marked E_{pl_1} in the Figure) that vary with L as expected for T-L plasmon type resonances. These resonances can only be excited with a parallel field as was confirmed by a simulation of the 5 unit cell tube with perpendicular excitation (marked '5T'). One of the series of 4-D snapshots (Collective Oscillation - $E_{pl_1} = 3.89\text{eV}$) shows how the charge density waves travel back and forth on the tube under sinusoidal excitation at the resonance frequency. There is a related plasmon resonance at a higher energy (E_{pl_2} at 4.76eV) for the 5-unit cell case. Thus we find split plasmon resonances for both cases - the 5 unit and 7 unit cell ones - with a much smaller split for the longer tube. The calculated velocities for the two T-L plasmons for the 5 unit cell case are $2.35 \times 10^6\text{m/s}$ and $2.87 \times 10^6\text{m/s}$, and they increase to $3.12 \times 10^6\text{m/s}$ and $3.29 \times 10^6\text{m/s}$ for the the 7 unit cell. The side view snapshots of the charge distribution in Figure 5 can now be used to discuss further the different characters of the resonances E_{e-} , E_{pl_1} and E_{pl_2} . The charge density for the single (quasi-particle) excitation (E_{e-}) is spread across the cross-section. In contrast, the plasmon excitations concentrate the charges around the periphery and at the ends of the tube as expected for a boson-type mode [7, 8, 10]. The split between the two plasmon frequencies can be interpreted as related to two different modes quantized around the periphery.

Given our interpretation of the peaks from 3.69eV to

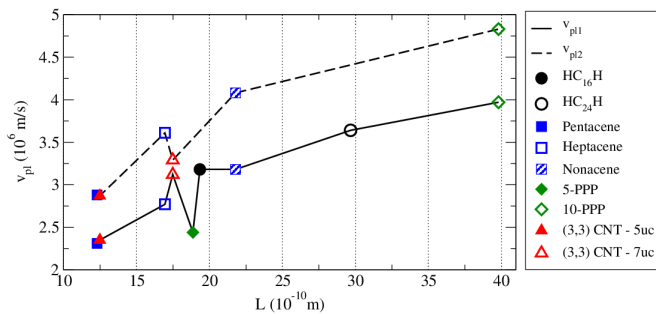


FIG. 6: Summary of plasmon velocities computed for all the 1-D carbon nanostructures using different lengths (numerical values are provided in supporting information document). Two main plasmon modes are represented (except for the carbyne and the 5-PPP cases). We note the universal monotonic increase of the plasmon velocities for longer structures, while the less regular behavior in the 15-20Å range (in particular for the 5-PPP and the 7-unit cell (3,3) SWCNT) is likely due to coupling effects between “band-to-band” transitions and the plasmons.

3.89eV as T-L plasmon resonances, we would expect a similar T-L plasmon resonance for the 3 unit cell case at a somewhat higher energy, where we see two peaks. As indicated earlier, this brings us to the expected energy of the π -plasmon, however, and a possible interpretation of the two peaks at 4.32eV and 4.81eV for the 3 unit cell tube is that the T-L plasmon and the π -plasmon are coupled.

Conclusions

This paper has simulated molecular absorption spectra employing accurate all-electron real-time TDDFT simulations. The range in size has been extended from small molecules such as C_2H_2 or benzene to carbon nano-structures that are equivalent to 1-D conductors with finite lengths. Excellent agreement with experimental spectra is obtained when such data is available.

We find universal features for all structures investigated which include carbon chains, narrow armchair and zigzag graphene nanoribbons (i.e. acenes and PPP), as well as short carbon nanotubes. All structures show collective plasmon oscillations characterized by resonant frequencies that vary roughly inversely with the length of the structure. For the metallic structures (in our case only the SWCNTs) the plasmons are expected to be related to the T-L plasmons of infinitely long 1-D structures. Another notable characteristic is that the main plasmon resonance is split into two components due to transverse quantum confinement effects (except for the case of carbyne that presents two to three longitudinal resonance modes). The simulations allow vivid 4-D visualizations of the electron charge distributions for different types of resonant modes, which then provide more insights on their nature. As summarized in Figure 6, the velocity of plasmon propagation shows a monotonic increase with the length of the structure and it is expected that the plasmon velocity will asymptotically become independent of length. Further optimization of our present high performance computing techniques should allow the extension of the simulations to longer structures (up to tens of unit cells for SWCNT), and lead to accurate predicted data that will guide future photonic and electronic applications of nanostructures over a wide frequency range, from visible to terahertz.

Supplementary information

The supplementary document to this article includes detailed information about the theoretical models and numerical methods used in this study, additional information data about the π and $\pi + \sigma$ resonances in SWCNT, and a table of numerical values for the plasmon velocities.

-
- [1] Stockman, M.I.; Nanoplasmonics: The physics behind the applications, *Physics Today*, 64 (2), 39-44 (2011).
 - [2] Halas, N.J.; Connecting the dots: Reinventing optics for nanoscale dimensions, *PNAS* 106, 3463 (2009).
 - [3] Novotny, L.; Van Hulst, N.; Antennas for light, *Nature Photonics*, 5, 83 (2011).
 - [4] Cang, H.; Labno, A.; Lu, C.; Yin, X.; Liu, M.; Gladden, C.; Liu, Y.; Zhang, X.; Probing the electromagnetic field of a 15-nanometre hotspot by single molecule imaging, *Nature* 469, 385 (2011).
 - [5] Plasmonics, *Nature Nano.*, special focus issue, Jan. (2015).
 - [6] Kittel, C.; Introduction to Solid State Physics, *Eight Edition*, Wiley and Sons, New York (2005).
 - [7] Tomonaga, S.; Remarks on Bloch’s method of sound waves applied to many-fermion problems. *Prog. Theor. Phys.* 5, 544569 (1950).
 - [8] Luttinger, J. M.; An exactly soluble model of a many-fermion system, *J. Math. Phys.* 4, 11541162 (1963).
 - [9] Deshpande, V. K.; Bockrath, M.; Glazman L.; Yacoby, A.; Electron liquids and solids in one dimension, *Nature* 464, 209 (2010).
 - [10] Haldane, P. D. M.; Luttinger Liquid Theory I. Properties of the Luttinger Model and their extension to the general 1-D interacting spinless Fermi gas, *J. Phys. C* 14, 2585-2609 (1981).
 - [11] Egger, R.; Gogolin, A. G.; Effective Low-Energy Theory for Correlated Carbon Nanotubes; *Phys.Rev. Lett.* 79,

- 5082 (1997).
- [12] Kane, C.; Balents, L.; Fisher, P.A.; Coulomb Interactions and Mesoscopic Effects in Carbon Nanotubes; *Phys. Rev. Lett.* 79, 5086 (1997).
- [13] Auslaender, D.M.; Yacoby, A.; de Picciotto, R.; Baldwin, K. W.; Pfeiffer, L. N.; West, K. W.; Tunneling spectroscopy of the elementary excitations in a one-dimensional wire; *Science* 295, 825-828 (2002).
- [14] Saito, R.; Dresselhaus, G.; Dresselhaus, M.S.; Physical Properties of Carbon nanotubes; *Imperial College Press*, London, 1998.
- [15] Bockrath, M.; Cobden, D. H.; Rinzler, A. G.; Smalley, R. E.; Balents, L.; McEuen, P. L.; Luttinger-liquid behaviour in Carbon Nanotubes; *Nature* 397, 598-601 (1999).
- [16] Yao, Z.; Postma, H. W.; Balents, L.; Dekker, C.; Carbon nanotube molecular junctions; *Nature* 402, 273-276 (1999).
- [17] Ishii, H.; Kataura, H.; Shiozawa, H.; Yoshioka, H.; Otsubo, H.; Takayama, Y.; Miyahara, T.; Suzuki, S.; Achiba, Y.; Nakatake, M.; Narimura, T.; Higashiguchi, M.; Shimada, K.; Namatame, H.; Taniguchi, M.; Direct Observation of Tomonaga-Luttinger-liquid states in carbon nanotubes at low temperatures; *Nature* 426, 540-544 (2003).
- [18] Zhang ,Q.; Haroz, E. H.; Jin, Z.; Ren, L.; Wang, X.; Arvidson, R. S.; Lüttge, A.; Kono, J.; Plasmonic Nature of the Terahertz Conductivity Peak in Single-Wall Carbon Nanotubes, *Nano Lett.*, 13 (12), 5991-5996 (2013).
- [19] Zhong Z.; Gabor, N.; Sharping, J.; Gaeta, A.; McEuen, P.; Terahertz time-domain measurement of ballistic electron resonance in a single-walled carbon nanotube, *Nature Nanotech.*, 3, 201205 (2008).
- [20] Hanson, G. W.; Current on an Infinitely-Long Carbon Nanotube Antenna Excited by a Gap Generator; *IEEE Transactions on Antennas and Propagation*, 54, 76-81 (2006).
- [21] Blumenstein, C.; Schäfer, J.; Mietke, S.; Meyer, S.; Dollinger, A.; Lochner, M.; Cui, X.Y.; Patthey, L.; Matzdorf, R.; Claessen, R.; Atomically controlled quantum chains hosting a Tomonaga-Luttinger liquid, *Nature Physics* 7, 776-780 (2011).
- [22] Burke, P.J.; Luttinger Liquid Theory as a Model of the Gigahertz Electrical Properties of Carbon Nanotubes, *IEEE Trans. Nanotechnol.* 1, 129 (2002).
- [23] Bockrath. M. W.; Carbon Nanotubes: Electrons in One Dimension; *PhD thesis*, University of California, Berkeley, 1999.
- [24] The resonance frequency is related to the phase velocity of the resonant wave. For the basic T-L model the waves are non-dispersive (i.e. the phase velocity is equal to the group velocity). This is no longer true for the short structures simulated here. We derive the plasmon phase velocity from the standard formula $v = \omega/k$ where ω is the angular frequency and $k = 2\pi/\lambda$ is the wavevector. At resonance $L = \lambda/2$. This convention allows us to show the trend of plasmon velocity versus length. As the length of the structure increases the dispersion relation will asymptotically become linear and the group velocity will become equal to the phase velocity.
- [25] Runge, E.; Gross, E. K. U.; Density-Functional Theory for Time-Dependent Systems, *Phys. Rev. Lett.*, 52, 997-1000, (1984).
- [26] Fundamentals of Time-Dependent Density Functional Theory; Editors: Marques M. A. L.; Maitra N. T.; Nogueira, F. M. S.; Gross, E. K. U.; Rubio, A.; *Lecture Notes in Physics* 837, Springer Verlag, (2012).
- [27] Yabana K.; Bertsch, G. F.; Time-dependent local-density approximation in real time, *Phys. Rev. B*, 54, 4484 (1996).
- [28] Yabana, K.; Nakatsukasa, T.; Iwata, J.-I.; Bertsch, G. F.; Real-time, real-space implementation of the linear response time-dependent density-functional theory, *Phys. Stat. Sol. (b)*, 243, No. 5, 1121-1138 (2006).
- [29] Polizzi, E.; Density-matrix-based algorithm for solving eigenvalue problems, *Phys. Rev. B*, 79, 115112, (2009).
- [30] The FEAST eigensolver, <http://www.feast-solver.org>
- [31] Levin, A.; Zhang, D.; Polizzi, E.; FEAST fundamental framework for electronic structure calculations: Reformulation and solution of the muffin-tin problem, *Comput. Phys. Comm.*, 183, I11, 23702375 (2012).
- [32] Gavin, B.; Polizzi, E.; Non-linear eigensolver-based alternative to traditional SCF methods, *J. Chem. Phys.*, 138, 194101 (2013).
- [33] Chen, Z.; Polizzi, E.; Spectral-based propagation schemes for time-dependent quantum systems with application to carbon nanotubes, *Phys. Rev. B*, 82, 205410 (2010).
- [34] Chalifoux, W.; Tykwinski, R.; Synthesis of Polyynes to Model the sp-Carbon Allotrope Carbyne, *Nature Chem.*, 2, 967971 (2010).
- [35] Artyukhov, V.I.; Liu, M.; Yakobson, B.I.; Mechanically Induced Metal Insulator Transition in Carbyne, *Nano Letters*, 14, 4224-4229 (2014).
- [36] Yabana, K.; Bertsch, G.F.; Optical response of small carbon clusters, *Zeitschrift fr Physik D Atoms, Molecules and Clusters*, 42, 13, 219-225 (1997).
- [37] Berkus, C.; Reinhard, P.-G.; Suraud, E.; Dynamical Effects in the Optical Response of Carbon Chains; *Int. J. Mol. Sci.*, 3, 69-75 (2002).
- [38] Huang, Y-H.; Lin, K-M.; Leung, T.C.; Chan, C.T.; Plasmonlike resonances in atomic chains: A time-dependent density-functional theory study, *Phys. Rev. B*, 90, 075418 (2014).
- [39] Schermann, G.; Grosser, T.; Hampel, F.; Hirsch, A.; Dicyanopolyynes : a homologous series of end-capped linear sp carbon, *Chem. Eur. J.* 3, N7 1105-1112, (1997).
- [40] NIST Computational Chemistry Comparison and Benchmark Database; *NIST Standard Reference Database*, Number 101, Release 16a, August 2013, Editor: Russell D. Johnson III <http://cccbdb.nist.gov/>
- [41] Zhang, J-L.; Wu, W-P.; Wang L-B.; Cao Z-X.; Structural and Spectroscopic Properties of Linear Carbon Chains $NC_{2n}N$ and $HC_{2n+1}N$ ($n = 1 \sim 10$), *Chinese J. Struct. Chem.*, 24, 18, 885-894 (2005).
- [42] Horny L.; Petraco, N. D. K.; Pak, C.; Schaefer, H. F. III; What is the nature of polyacetylene neutral and anionic chains $HC_{2n}H$ and $HC_{2n}H$ ($n = 6 - 12$) that have recently been observed?, *J. Am. Chem. Soc.*, 124, 5861-5864, (2002).
- [43] Koryta R.; Xenioti, D.; Schmitteckert, P.; Alouani M.; Evers, F.; Signature of the Dirac cone in the properties of linear oligoacenes, *Nature Communications*, 5, 10.1038/ncomms6000 (2014).
- [44] Lopata, K.; Reslan, R.; Kowalska, M.; Neuhauser, D.; Govind, N.; Kowalski, K.; Excited-state studies of polyacenes: a comparative picture using EOMCCSD, CR-

- EOMCCSD(T), range-separated (LR/RT)-TDDFT, TD-PM3, and TD-ZINDO, *J. Chem. Theory Comput.*, 7, 36863693 (2011).
- [45] Freidel R. A.; Orchin M.; *Ultraviolet Spectra of Aromatic Compounds*, Wiley, New York, 1951.
- [46] Sato, N.; Inokuchi, N.; Silinsh, E. A.; Reevaluation of electronic polarization energies in organic molecular crystals, *Chem. Phys.*, 115, 269-277 (1987).
- [47] Cocchi, C.; Prezzi, D.; Ruini, A.; Benassi, E.; Caldas, M. J.; Corni, S.; Molinari, E.; Optical Excitations and Field Enhancement in Short Graphene Nanoribbons, *The Journal of Physical Chemistry Letters*, 3, 924-929 (2012).
- [48] Ambrosch-Draxl, C.; Majewski, J. A.; Vogl, P.; Leising, G.; First-principles studies of the structural and optical properties of crystalline poly-(paraphenylene), *Phys. Rev. B*, 51, 9668-9676 (1995).
- [49] Tabata, M.; Satoht, M.; Kaneto, K.; Yoshino, K.; Electrochemical n-type doping of poly(p-phenylene) film, *J. Phys. C: Solid State Phys.*, 19, 101-105 (1986).
- [50] Kramberger C.; Hambach, R.; Giorgetti, C.; Rümeli, M. H.; Knupfer, M.; Fink, J.; Büchner, B.; Reining, L.; Einarsson, E.; Maruyama, S.; Sottile, F.; Hannewald, K.; Olevano, V.; Marinopoulos, A. G.; Pichler, T.; Linear Plasmon Dispersion in Single-Wall Carbon Nanotubes and the Collective Excitation Spectrum of Graphene, *Phys. Rev. Lett.*, 100, 119803 (2008).
- [51] Kataura, H.; Kumazawa, Y.; Maniwa, Y.; Umezu, I.; Suzuki, S.; Ohtsuka Y.; Achiba, Y.; Optical Properties of Single-Wall Carbon Nanotubes, *Synthetic Metals* 103, 2555-2558 (1999).
- [52] Murakami, Y.; Einarsson, E.; Edamura, T.; Maruyama, S.; Polarization Dependence of the Optical Absorption of Single-Walled Carbon Nanotubes, *Phys. Rev. Lett.*, 94, 087402 (2005).
- [53] Spataru, C.D.; Ismail-Beigi, S.; Benedict, L. X.; Louie, S.G.; Excitonic Effects and Optical Spectra of Single-Walled Carbon Nanotubes, *Phys. Rev. Lett.*, 92, 077402 (2004).

Supporting Information for:

**Universal nature of collective plasmonic excitations in finite 1-D
carbon-based nanostructures**

Eric Polizzi, Sigfrid Yngvesson

Department of Electrical and Computer Engineering, University of
Massachusetts, Amherst

Contents

1	Methods - Summary	2
1.1	Ground-state calculations.	2
1.2	Excited-state calculations.	2
2	Methods - Practical considerations with applications to benzene	3
2.1	Real-space discretization	3
2.2	Real-time calculations and absorption spectra	4
3	Supplementary Figure for SWCNT	7
4	Supplementary Table for Plasmon velocities	7

1 Methods - Summary

From physics to algorithms, an account of the multi-step modeling process used by our in-house real-space and real-time NESSIE simulator is summarized in the following.

1.1 Ground-state calculations.

Our physical model to calculate the ground-state wave functions is at the level of Density Functional Theory (DFT) associated with the Kohn-Sham equations. For this study, the many body exchange-correlation term is defined using a standard local density approximation (LDA) formula [1]. The electronic Hamiltonian accounts for the full core potential (also called all-electron calculations). In contrast to pseudopotential methods in particular, this approach provides higher accuracy, consistency, and higher locality in the discretization stage with better potentiality for parallelism. The number of electrons in our simulations range from a few tens for small molecules (e.g. 42 electrons for benzene) to a few hundreds for most of the nanostructures considered here (e.g. 552 electrons for the (3,3) SWCNT with 7 unit cells). The finite element method is used to discretize the Hamiltonian system using tetrahedral elements with either quadratic P2 or cubic P3 basis functions (P2 is preferred for our TDDFT linear response simulations using weak perturbation – it is computationally less expensive and essentially provides the same results). The real-space simulation domain is taken large enough to minimize any unwanted scattering from artificial boundaries. More details on our FEM real-space mesh approach are presented in the next Section. In turn, the significant challenges posed by the NESSIE’s large-sparse matrix computations resulting from the real-space mesh discretization have been addressed recently with the development of our FEAST eigensolver [2, 3]. FEAST has considerably broadened the perspectives for enabling high-performance parallel large-scale calculations. In particular, we operate FEAST beyond the current “black-box” solver by considering a fundamental redesign of the electronic structure numerical modeling, including: (i) a reformulation of the real-space muffin-tin domain-decomposition problem for solving the first-principle all-electron problem exactly [4], (ii) a fundamental non-linear FEAST numerical technique for addressing the self-consistent (SCF) DFT ground-state problem that represents a robust alternative to traditional SCF methods using iterative procedure with density mixing schemes [5].

1.2 Excited-state calculations.

Within the real-time TDDFT framework, all the occupied N_e ground-state wave functions $\{\phi_1, \dots, \phi_{N_e}\}$ are propagated (non-linearly) in time by solving a time-dependent Kohn-Sham type equation. The absorption spectrum is obtained after a short polarized impulse is applied in any given direction η (e.g. x, y or z) of the molecular system i.e. $\psi_j(\mathbf{r}, t = 0^+) = \exp(-ik\eta)\phi_j(\mathbf{r})$ [6]. Using the solution of the electron density at each time step i.e. $n(\mathbf{r}, t) = 2 \sum_{j=1}^{N_e} |\psi_j(\mathbf{r}, t)|^2$, the induced dipole can then be computed in the time-domain $d(t) = \int d\mathbf{r} n(\mathbf{r}, t)\eta$, and the imaginary part of its Fourier transform provides the dipole strength function and the absorption spectrum. Examples on the dipole variations and more details on the calculations of the dipole strength function are presented in the next Section. The real-time TDDFT technique is often used to address linear responses (e.g. using weak momentum k), but the framework can also generally address any forms of non-linear responses. In our simulations in particular, a longitudinal sinusoidal excitation is often used to observe the dynamics of the charge oscillations at a given resonance frequency. The real-time propagation is performed using either a conventional Crank-Nicolson (CN) scheme or a spectral decomposition technique where FEAST is used to diagonalize the time-dependent Hamiltonian at

each time step [7]. This FEAST spectral decomposition technique is well-suited for parallel computing, and it allows to consider larger time-steps in our simulations $\Delta_t = 20as$ (vs $\Delta_t = 2as$ using CN). The total simulation time that has been used varies between 10fs for the carbynes to 15fs for the SWCNTs.

2 Methods - Practical considerations with applications to benzene

Supplementary information on the modeling procedure used in NESSIE is provided here. We use the example of the benzene molecule.

2.1 Real-space discretization

As specified by an input file, our simulator NESSIE reads the atom coordinates, creates a 3D mesh using tetrahedra, and it builds the FEM Hamiltonian and mass (i.e. basis function overlap) matrices using quadratic P2 or cubic P3 precision.

The 3D FEM mesh is constructed using a muffin-tin decomposition technique that involves two steps: (i) a 3D atom-centered mesh which is highly refined around the nucleus to capture the full core potential, and (ii) a much coarser 3D interstitial mesh that connects all the atom-centered holes and extends to the computational domain boundary. Figure S1 illustrates the essence of our FEM muffin-tin domain decomposition for the benzene molecule. The size of the full 3D (reconstructed)

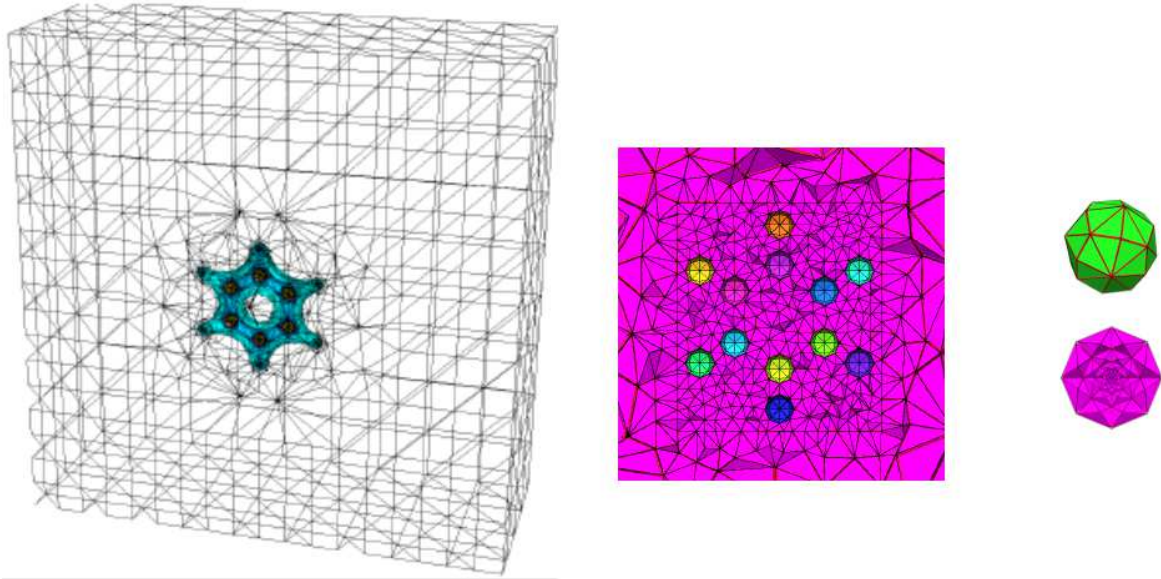


Figure S1: *Using a muffin-tin domain-decomposition method, the whole simulation domain Ω is separated into multiple atom-centered regions (i.e. muffins on the right) and one large interstitial region (on the left). The figure in the middle represents a 2D section of local finite element discretization using a coarse interstitial mesh (represented only partially here) connecting all of the atoms of a benzene molecule.*

sparse system matrix for benzene is $\sim 60K$ using P2, and $\sim 140K$ using P3. In TDDFT calculations using a weak perturbation, a P2 FEM basis provides results similar to P3. Table S1 reports the

	Carbyne		Acenes			PPP		SWCNT	
	HC ₁₆ H	HC ₂₄ H	Penta.	Hepta.	Nona.	5PPP	10PPP	5-unit	7-unit
# electrons	98	146	146	198	250	202	402	408	552
Size H matrix	65,357	93,115	138,926	180,272	223,813	191,643	368,133	302,282	393,410

Table S1: Hamiltonian system size P2 FEM discretization by NESSIE for various 1-D carbon nanostructures. The system matrices are very sparse with an average of 15 to 20 non-zero elements per row.

size of the resulting P2 FEM Hamiltonian system matrices and the total number of electrons for most of the 1-D carbon nanostructures we have considered in our simulations.

The real-space simulation domain Ω is taken large enough to minimize any unwanted scattering from artificial boundaries. The wave functions are set equal to zero at the boundaries (i.e. Dirichlet boundary conditions for Kohn-Sham), and radiative boundary conditions on the electrostatics potential are used for solving the Poisson equation. The coupled DFT-Kohn-Sham/LDA/Poisson problem is solved self-consistently using the non-linear version of the FEAST solver. In particular, the lowest $N_e/2$ states are computed (N_e denoting the number of electrons, and the factor 2 accounts for the spin).

2.2 Real-time calculations and absorption spectra

Two perturbations of the ground state solutions are considered in the simulation (i) a weak short impulse along a given direction (longitudinal or perpendicular to the structure), (ii) a weak sinusoidal stimulus at a given resonance frequency. In both cases, the ground-state occupied wave functions (i.e. electrons) need to evolve in time. At each new time step $t + \Delta_t$, the Poisson equation is solved, and the time-dependent ALDA Hamiltonian is updated. We are also making use of a simple corrector-predictor schemes to evaluate the Hamiltonian at $t + \Delta_t/2$. For the real-time propagation, two strategies have been used: (i) a Crank-Nicolson (CN) scheme that requires solving a linear system at each time step (number of right-hand-side is equal to $N_e/2$); (ii) a spectral decomposition scheme that requires the partial diagonalization of the large Hamiltonian at each time step. The latter direct diagonalization technique can become a viable alternative to CN (i.e. potentially capable of both higher-scalability and better accuracy) only if used within a parallel computing environment and by taking advantage of various intrinsic properties of the FEAST solver (e.g. the eigenvector subspace computed in the current time-step can be used as a good initial guess for computing the next one).

Thereafter, at each time step we compute the 3d electron density (sum of amplitude square of the occupied wave functions that are propagated). The variation of the induced dipole is then computed relative to the dipole of the ground state and the center of mass $r_0 \equiv (x_0, y_0, z_0)$ of the nanostructure. For example, the response along the longitudinal z direction is given by:

$$\delta d_z(t) = \int_{\Omega} d\mathbf{r} (n(\mathbf{r}, t) - n(\mathbf{r}, 0))(z - z_0).$$

For the case of a short polarized impulse initial perturbation (using a weak momentum k), the dipole strength function S is obtained by taking the imaginary part of the Fourier transformation of the dipole moment, i.e.

$$S(E) = \frac{2mE}{\pi k \hbar^3} \Im \left\{ \int_0^T dt \delta d(t) e^{-iEt/\hbar} w(t) \right\},$$

where $w(t)$ represents a damping factor that introduces artificial dissipation for suppressing the noise in the Fourier transform (we choose $w(t) = e^{-\gamma t/T}$). Typically in our simulations, we set $\gamma = 3$, and $k = 0.01/L$ where L is the dimension of the computational domain along the polarization direction. For the example of the benzene molecule, Figure S2 presents the results obtained for the dipole variations and their associated absorption spectrum, after an excitation is applied along the three main directions of the molecule. The mean of the three solutions is plotted in Figure S3 and it can be quantitatively compared with the experimental data.

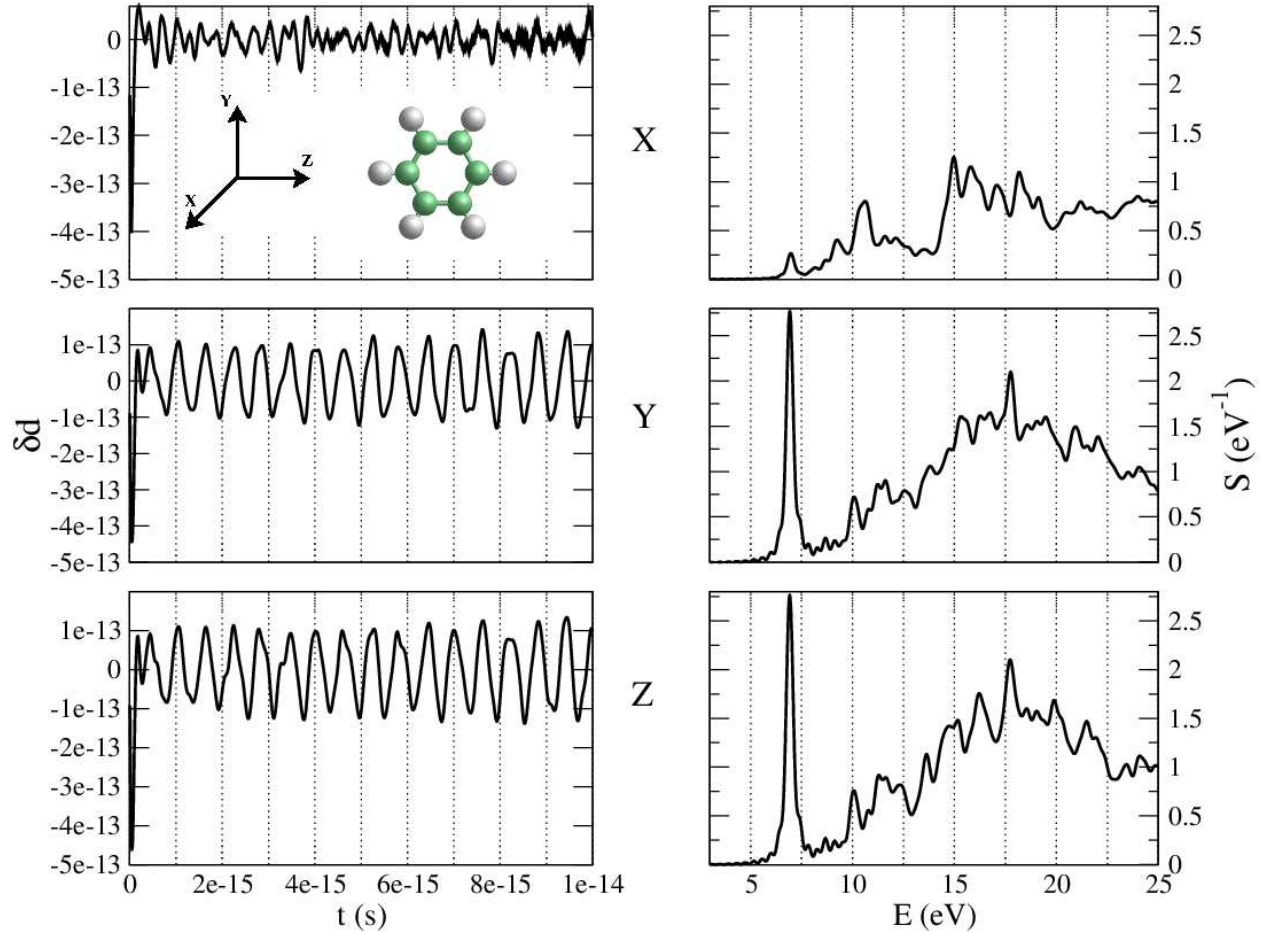


Figure S2: *Dipole variations and corresponding absorption spectrum after excitation along the three main direction of the benzene molecule. The CN scheme is used for real-time propagation with time-step $\Delta_t = 5\text{as}$ and a total time of 10fs (2000 time steps).*

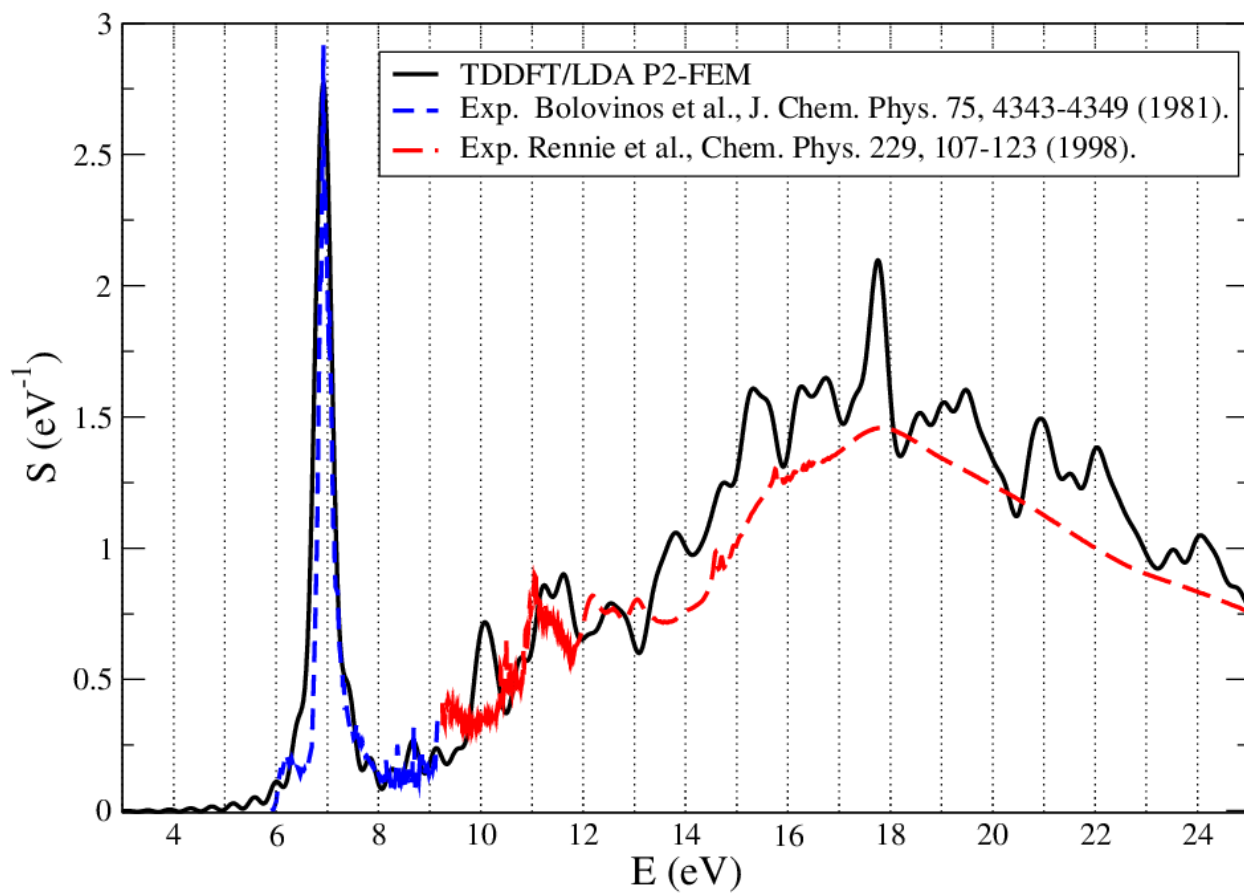


Figure S3: Calculated absorption spectrum of the benzene molecule using NESSIE and comparison with experimental data.

3 Supplementary Figure for SWCNT

Figure 5 shows the simulation results for a finite (3,3) armchair SWCNTs including the $\pi + \sigma$ bulk-type plasmon peak - broad band at $\sim 15\text{eV}$. We note that both π and $\pi + \sigma$ resonances for a perpendicular excitation are shifted to higher energy values in qualitative agreement with the experimental data (e.g. Kramberger C. et al., Phys. Rev. Lett., 100, 119803, 2008).

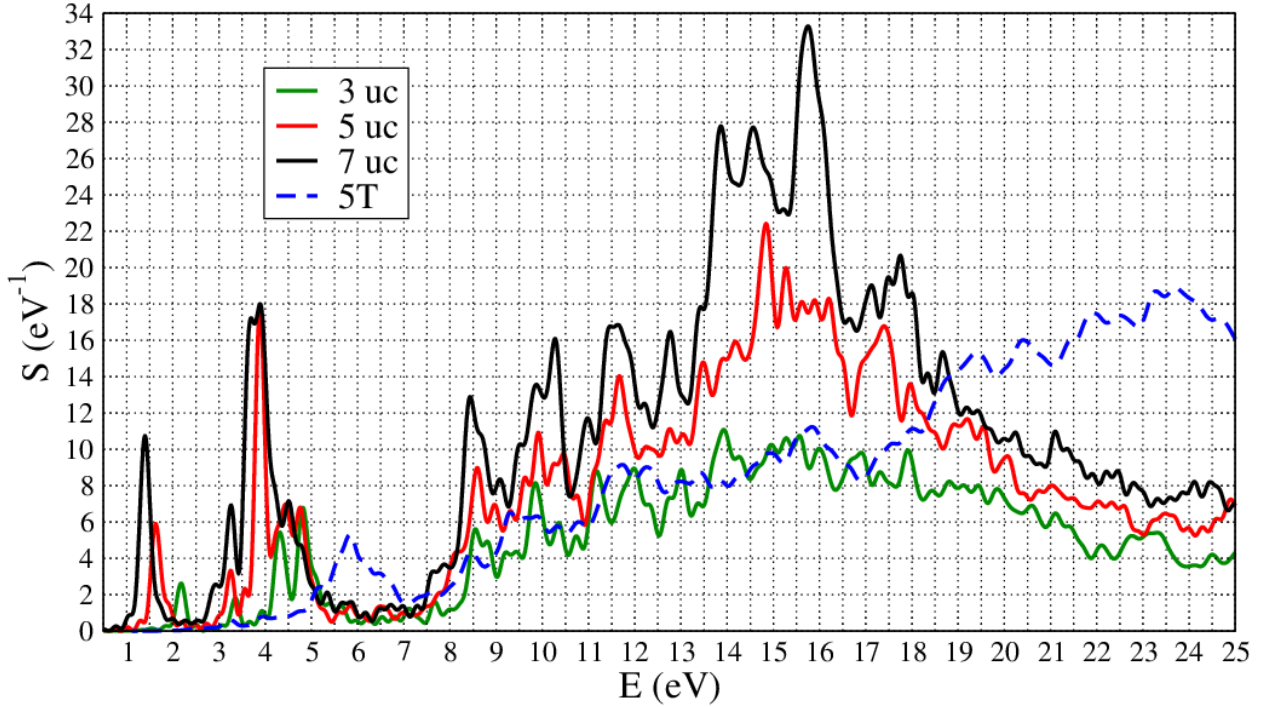


Figure S4: Calculated absorption spectra of the finite (3,3) armchair SWCNT with three different length 3, 5 and 7 unit cells (the C-C bond length is fixed at 1.44\AA and one additional carbon ring of type 'A' is added to the structures e.g. 'H-AB-AB-AB-A-H' for the 3 unit cells with Hydrogen termination). The '5T' curve indicates the result from an excitation in the perpendicular direction, all other results consider an excitation along the longitudinal direction of tube.

4 Supplementary Table for Plasmon velocities

	Carbyne		Acenes			PPP		SWCNT	
	HC ₁₆ H	HC ₂₄ H	Penta.	Hepta.	Nona.	5PPP	10PPP	5-unit	7-unit
L (\AA)	19.34	29.67	12.29	16.94	21.78	18.86	39.81	12.48	17.48
E_{pl_1} (eV)	3.40	2.53	3.88	3.38	3.02	2.67	2.06	3.89	3.69
v_{pl_1} (10^6m/s)	3.18	3.64	2.31	2.77	3.18	2.44	3.97	2.35	3.12
E_{pl_2} (eV)			4.84	4.41	3.87		2.51	4.76	3.89
v_{pl_2} (10^6m/s)			2.88	3.61	4.08		4.83	2.87	3.29

Table S2: Numerical values of T-L plasmon velocities computed for all the 1-D carbon nanostructures using different lengths. Two main plasmon modes are reported (except for the carbyne and the 5PPP cases).

References

- [1] Perdew, J.P.; Zunger, A.; Self-interaction correction to density-functional approximation for many-electron system, *Phys. Rev. B*, 23, 5048-5079 (1981).
- [2] Polizzi, E.; Density-matrix-based algorithm for solving eigenvalue problems, *Phys. Rev. B*, 79, 115112, (2009).
- [3] The FEAST eigensolver, <http://www.feast-solver.org>
- [4] Levin, A.; Zhang, D.; Polizzi, E.; FEAST fundamental framework for electronic structure calculations: Reformulation and solution of the muffin-tin problem, *Comput. Phys. Comm.*, 183, I11, 2370–2375 (2012).
- [5] Gavin, B.; Polizzi, E.; Non-linear eigensolver-based alternative to traditional SCF methods, *J. Chem. Phys.*, 138, 194101 (2013).
- [6] Yabana, K.; Nakatsukasa, T.; Iwata, J.-I.; Bertsch, G. F.; Real-time, real-space implementation of the linear response time-dependent density-functional theory, *Phys. Stat. Sol. (b)*, 243, No. 5 , 1121-1138 (2006).
- [7] Chen, Z.; Polizzi, E.; Spectral-based propagation schemes for time-dependent quantum systems with application to carbon nanotubes, *Phys. Rev. B*, 82, 205410 (2010).